letters to nature

···

Testing the thermodynamic approach to granular matter with a numerical model of a decisive experiment

Hernán A. Makse* & **Jorge Kurchan**†

* *Levich Institute and Physics Department, City College of the City University of New York, New York, New York 10031, USA*
† *PMMH, Ecole Supérieure de Physique et Chimie Industrielles, 10 rue Vauquelin, 75231 Paris, France*

···

Edwards has proposed[1–3] a thermodynamic description of dense, slowly flowing granular matter, in which the grains (the 'atoms' of the system) interact with inelastic forces and enduring contacts. In Edwards' ensemble—one of the very few generalizations of standard statistical mechanics—thermodynamic quantities are computed as flat averages over configurations in which the grains are static or jammed, leading to a natural definition of configurational temperature. But the approach is not justified from first principles and hence, in the absence of explicit tests of its validity, has not been widely accepted. Here we report a numerical experiment involving a realistic model of slowly sheared granular matter; our results strongly support the thermodynamic description. Considering particles of different sizes in a slowly sheared dense granular system, we extract an effective temperature from a relation connecting their diffusivity and mobility. We then perform an explicit computation to show that the effective temperature measured from this relation coincides with the Edwards configurational temperature. Our approach, which is specifically conceived to be reproducible in the laboratory, may thus render the Edwards temperature accessible to experiments.

Consider a 'tracer' body of arbitrary shape immersed in a liquid in thermal equilibrium. As a consequence of the irregular bombardment by the particles of the surrounding liquid, the tracer performs a diffusive, fluctuating 'brownian' motion. The motion is unbiased, and for large times the average square of the displacement is given by $\langle |x(t) - x(0)|^2 \rangle = 2Dt$, where D is the diffusivity. On the other hand, if we pull gently on the tracer with a constant force f, the liquid responds with a viscous, dissipative force. The averaged displacement after a large time is $\langle [x(t) - x(0)] \rangle = f\chi t$, where χ is the mobility. Clearly, the same liquid molecules are responsible both for the fluctuations and for the dissipation. Although both D and χ strongly depend on the shape and size of the tracer, they turn out to be always related by the Einstein relation $D/\chi = T$ (a form of the fluctuation–dissipation theorem), where T is the temperature of the liquid. Conversely, if in a fluid of unknown properties we find that several tracers (of different sizes, for instance) having different diffusivities and mobilities yield the same ratio $D/\chi = T$, we may take this as a strong evidence for thermalization at temperature T.

The Einstein relation is strictly valid for an equilibrium thermal system. However, recent analytic schemes for out-of-equilibrium glassy systems have shown that the Einstein relation gives rise to a well-defined 'effective temperature' which is different from the bath temperature and governs the heat flow and the slow components of fluctuations and responses of all observables[4,5]. The existence of an effective temperature with a thermodynamic meaning suggests a hidden form of 'ergodicity' for the slow modes of relaxation, which turns out to be closely related to Edwards' statistical ideas[1] for systems undergoing slow compaction. Explicit checks of this approach have been made so far within the mean-field/mode-coupling models of the glass transition[5], as well as for schematic finite-dimensional models of glassy systems[6–10].

On the experimental side, recently Nowak *et al.*[11] studied in detail the density fluctuations in a vibrated granular material, and proposed that these fluctuations should reflect an underlying thermodynamics, much as they do in an ordinary thermal system. However, as far as the actual verification of the granular thermodynamics was concerned, the evidence they found was negative: we shall discuss below some possible reasons for this. On the other hand, although Edwards' thermodynamics was originally formulated for granular matter, it has never been tested in realistic models of granular materials, characterized by the fact that energy is supplied by external driving (through, for instance, shear) and dissipated by inelastic collisions and slippage between the grains—a very different heat exchange mechanism from that of a thermal bath in a molecular system. In order to test the existence of an effective temperature with a thermodynamic meaning for dense, slowly moving granular matter, we perform, with a realistic numerical model, a diffusion-mobility experiment in conditions that can be reproduced in the laboratory. In the model, deformable spherical grains interact with one another via nonlinear elastic Hertz normal forces, nonlinear elastic and path-dependent Mindlin transverse forces, dissipative viscous damping force terms proportional to the relative normal and angular velocities, and via sliding friction with friction coefficient μ (see Methods 'Microscopic model'; refs 12–14).

We perform molecular dynamics (MD) simulations (also known as discrete element methods, DEM)[13–16] for a binary system of large and small spheres in a periodic three-dimensional cell. We apply a gentle simple shear flow at constant volume in the y-direction taking care that the gradient of the velocity along z is uniform (see Methods 'MD simulation'). We focus our study on the slow shear rate, where the system is always close to jamming, but moves just barely enough to avoid stick-slip motion[17]. After a transient of the order of the inverse shear rate, we start measuring the spontaneous $\langle |x(t) - x(0)|^2 \rangle$ and force-induced displacements $\langle [x(t) - x(0)] \rangle / f$ along the x-direction for two types of particles. To measure
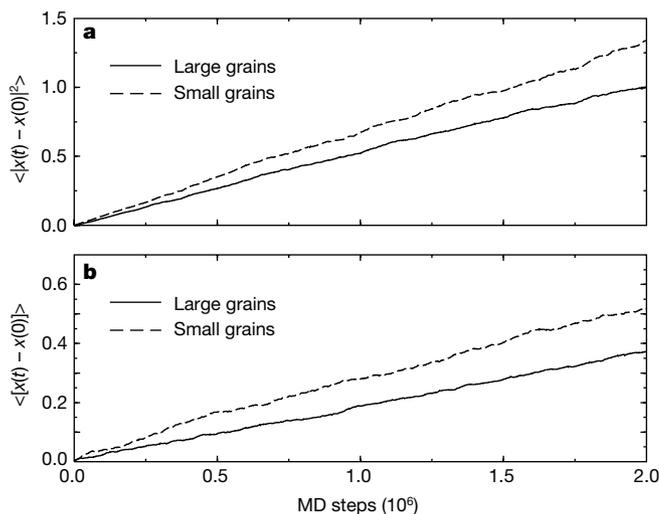

Figure 1 Diffusion (**a**) and response function (**b**) for the large and small particles in a sheared granular material measured perpendicular to the shear plane as a function of time in MD steps. Both quantities depend linearly on time at the late stages of the evolution. The response function is measured by applying a constant force f in the x-direction to each type of particle. Averages are taken over 30 realizations. The obtained diffusivities and mobilities depend on the particles size as expected. The slow frictional flow regime of interest in this study is accessed for shear rates $\dot{\gamma} \approx 10^{-3}$. The external pressure and mean solid fraction are large enough (~ 10 MPa and 0.66, respectively), and the average coordination number is high enough (typically ~ 7), that deformation and elasticity of the particles play the dominant role in the slow dynamics. The density of particles is uniform throughout the sample. The contacts between particles are enduring, and the internal stresses in the system are transmitted via a network of 'force chains'[24,25].

$\langle[x(t) - x(0)]\rangle/f$ we apply an external small constant force ($f \approx 10^{-2}$ times the mean value of the contact forces) to the large and small particles separately and monitor their displacements as a function of time, averaging over all the small and large particles, respectively. The results are shown in Fig. 1. We notice that the diffusivities and the mobilities are different for the two type of particles, as expected. However, when we draw the parametric plot of $\langle|x(t) - x(0)|^2\rangle$ versus $\langle[x(t) - x(0)]\rangle/f$ (Fig. 2) we find parallel straight lines for large timescales, implying an extended Einstein relation:

$$\langle|x(t) - x(0)|^2\rangle = 2\,T_{\text{eff}} \frac{\langle[x(t) - x(0)]\rangle}{f} \qquad (1)$$

valid for both particles with the same 'effective temperature' T_{eff} for large timescales. This suggests that T_{eff} can be considered to be the temperature of the slow modes.

We also repeat the numerical experiment for a system of Hertz spheres without transverse forces ($\mu = 0$: experimental realizations of elastic spheres interacting with normal forces (contact and viscous forces) but without sliding friction are foams and compressed emulsions[18–20]), and find that T_{eff} is well defined at long timescales for this case as well (see Fig. 2). Thus, our results suggest that the validity of an effective temperature for long-scale displacements (larger than a fraction of the particle size) holds in the presence of viscous forces between grains or even of a sliding threshold (Coulomb's law).

The existence of a single temperature is an instance of the 'zeroth law' of thermodynamics, for which we find positive evidence here, at variance with the experimental result of Nowak *et al.*[11]. Three possible reasons for the apparent violation of the 'zeroth law' in their experiments are (1) the effect of an unknown height-dependent pressure (as pointed out by the authors), (2) a rather high tapping amplitude (a well-defined T_{eff} is only to be expected in the high compaction limit, ref. 5), and (3) the fact that the density fluctuations considered are integrated over all frequencies, thus including, unlike the present work, also 'fast' relaxations.

Next, we treat the question whether it is possible to relate the effective temperature obtained above to the thermodynamic construction of out-of-equilibrium systems proposed by Edwards. While in the Boltzmann–Gibbs construction of statistical mechanics one assumes that the physical quantities are obtained as averages over all possible configurations, the Edwards ensemble consists of only the jammed (blocked or static) configurations at the appropriate energy and volume. The strong 'ergodic' hypothesis is that all jammed configurations of a given volume and energy can be taken to have equal statistical weights. This formulation leads to a configurational entropy $S_{\text{Edw}}(E, V) = \ln\Omega_{\text{Edw}}(E, V)$, where Ω_{Edw} is the number of jammed configurations, and the corresponding configurational temperature $T_{\text{Edw}}^{-1} = \partial S_{\text{Edw}}/\partial E$ and compactivity $X_{\text{Edw}}^{-1} = \partial S_{\text{Edw}}/\partial V$.

In order to calculate T_{Edw} and compare it with the obtained T_{eff}, we need to count the number of jammed configurations at a given energy and volume (for this calculation we concentrate on the case without tangential forces and sliding friction, in order to avoid path dependency which would lead to an ambiguity in the definition of jammed configurations—see below). Counting directly all jammed configurations is impossible, except for small systems. To do it in practice, we resort here to an indirect 'auxiliary model' method[7] suitably modified to the case of deformable grains. It consists of computing, using any standard method (Monte Carlo, MD, and so on), the equilibrium properties of the granular system
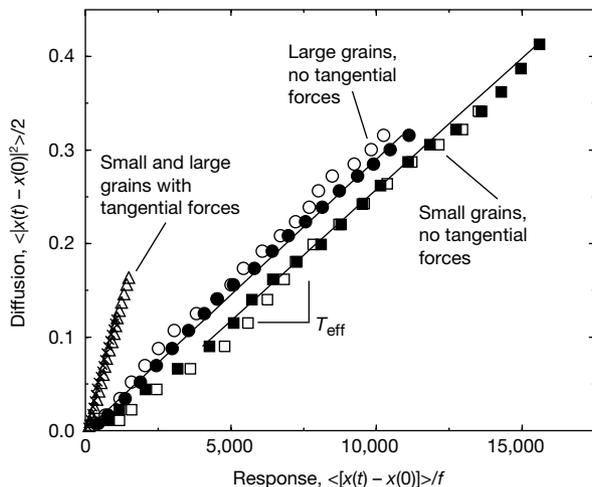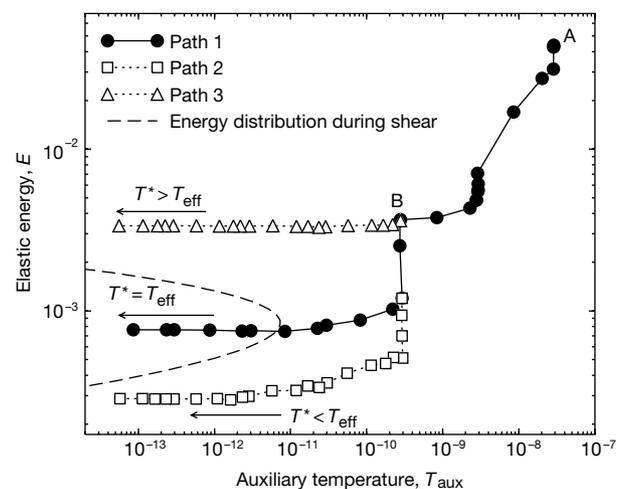

Figure 2 Parametric plot of diffusion versus response function for small and large grains interacting with tangential forces and without tangential forces (Coulomb frictionless). The fitting at long timescales shows the existence of a well defined effective temperature which is the same for small and large grains: $T_{\text{eff}} = 2.8 \times 10^{-5}$ for grains without transverse forces, and $T_{\text{eff}} = 1.2 \times 10^{-4}$ for grains with Mindlin transverse forces and Coulomb friction. These effective temperatures are about 10^{14} times kT at room temperature, as expected[26]. We calculate the response function for several small external fields and find the same temperature, indicating that we are in the linear response regime. Plotted are results for a system without transverse forces using: $f = 1.7 \times 10^{-5}$ (small grains, open squares; large grains, open circles) and $f = 2.6 \times 10^{-5}$ (small grains, filled squares; large grains, filled circles). For a system with tangential forces and Coulomb friction we show the case $f = 6 \times 10^{-5}$ (small grains, triangles; large grains, crosses). For small timescales (fast rearrangements, not seen in this figure) this fluctuation-dissipation plot yields no evidence for a well-defined temperature. We expect this result, because the fast motion of the grains depends on the microscopic interactions dominated by inelastic collisions between grains. This two-relaxation model is analogous to that found for glasses, although in the case of glasses a well-defined temperature is also found for the fast rearrangements of the particles[4].

Figure 3 Annealing procedure to calculate T_{Edw} at different elastic compressional energies. We plot the elastic energy versus T_{aux} during the annealing, together with the distribution of elastic energies obtained during shear (dashed curve, mean value $\langle E \rangle = 8.4 \times 10^{-4}$). We equilibrate the system for 40×10^6 iterations at A: ($T^* = 3.4 \times 10^{-2}$, $T_{\text{aux}} = 3 \times 10^{-8}$). We then anneal slowly both temperatures until B: ($T^* = 3.4 \times 10^{-4}$, $T_{\text{aux}} = 3 \times 10^{-10}$), where we split the trajectory into three paths in the (T^*, T_{aux}) plane. Path 1: we anneal $T_{\text{aux}} \to 0$ and $T^* \to 2.8 \times 10^{-5}$ which corresponds to T_{eff} obtained during shear (Fig. 2). Path 2: we anneal $T_{\text{aux}} \to 0$ and $T^* \to 3.4 \times 10^{-6}$. Path 3: we anneal $T_{\text{aux}} \to 0$ but keep $T^* = 3.4 \times 10^{-4}$ constant. When we set $T^* = T_{\text{eff}}$ (Path 1), the final elastic compressional energy value when $T_{\text{aux}} \to 0$ falls inside the distribution of energies obtained during shear, and it is very close to the mean value of the elastic energy during shear $\langle E \rangle$. This proves that $T_{\text{eff}} = T_{\text{Edw}}$ under the numerical accuracy of the simulations. For other values of $T^* \neq T_{\text{eff}}$, the final E falls out of the distribution obtained during shear (paths 2 and 3). We also follow different trajectories (not shown in the figure) to $T^* \to 2.8 \times 10^{-5}$, $T_{\text{aux}} \to 0$ and find the same results, indicating that our procedure is independent of the annealing path.

 615

in the periodic cell with the modified partition function $\Sigma \exp[-E/T^{\star} - E_{jammed}/T_{aux}]$, where E is the elastic compressional potential energy leading to the Hertz contact force, and $E_{jammed} \approx \Sigma_a |\mathbf{F}_a|^2$, with $\mathbf{F}_a$ the total contact force exerted on particle a by its neighbours. Thus, the dynamical system studied previously via the Einstein relation is now augmented by a temperature $T^{\star}$ setting the mean elastic energy per grain, plus an auxiliary temperature, T_{aux}, which relates to the (artificial) term E_{jammed} which selects, in the limit $T_{aux} \rightarrow 0$, the configurations where the grains are jammed ($E_{jammed} \rightarrow 0$).

It can be shown, although it may not be immediately obvious, that the following protocol yields the correct Edwards temperature at energy E. We start by equilibrating the system at high temperatures (T_{aux} and $T^{\star} \approx \infty$), and anneal slowly the value of T_{aux} to zero while tuning $T^{\star}$ so as to achieve a given final elastic potential energy E. At the end of the procedure ($T_{aux} \rightarrow 0$), we read Edwards' temperature as $T_{Edw}(E) = T^{\star}(E)$. This simulation is performed with the same system parameters as in the previous dynamical simulations within the shearing cell, but without viscous internal dissipation and external shear. We note that the procedure is a calculational trick, and it does not correspond to any real experimental protocol.

In Fig. 3 we plot the elastic compressional energy as a function of T_{aux} for three annealing protocols using different values of $T^{\star}$; we also show the distribution of compressional elastic energies obtained during the shearing experiments. The y-intercept of each annealing curve gives, as mentioned above, the value of E at $T_{Edw} = T^{\star}$. Only when we set $T^{\star}$ equal to T_{eff} (as obtained through the Einstein relation in the shearing cell), do we find that the final E coincides, within the accuracy of the simulations, with the mean elastic compressional potential energy of the system under shear (Fig. 3). This shows the agreement between Edwards' T_{Edw} and the effective temperature T_{eff}.

We conclude with some remarks. (1) Because the jammed configurations are the same whatever the inter-grain dissipation coefficient, Edwards' ensemble (and hence its temperature) is insensitive to viscous dissipation, as long as we are in the slow flow regime of interest in this study. (2) But tangential forces and sliding friction may or may not block certain configurations, depending on how they are accessed: the ensemble of jammed configurations is then ill-defined. We have not tried to construct a suitable ensemble for this case, but content ourselves with the observation that T_{eff} is also in this case independent of the particle size (Fig. 2)—our results suggest that thermodynamic concepts still apply, but the relevant ensemble for frictional systems necessarily goes beyond Edwards' construction as it stands. (3) We have tested the validity of the thermodynamics in an ideal homogeneous system with periodic boundary conditions by explicitly avoiding structural features of dense granular flows such as inhomogeneities and shear bands (by imposing a uniform shear rate), segregation of the species or long-range order[21,22]. Thus, the experimental test of our computational results may be complicated by, for instance, the formation of shear bands which tend to be present in physical systems. Even though it remains to be seen whether the thermodynamic picture may account for these highly nonlinear and dissipative effects, our ideal system may prove to be useful in deriving constitutive relations to be used in macroscopic theories of slow granular flows.

We have performed numerically a diffusion-mobility experiment with a dense, slowly sheared granular system specially designed to be a 'dress rehearsal' for the real laboratory experiment. The non-dependence of T_{eff} on the tracer size provides strong evidence for an underlying thermodynamics. We have then independently computed the configurational temperature T_{Edw} based on the entropy of jammed configurations and verified that it coincides with T_{eff}—thus supporting Edwards' statistical mechanical ideas. This last step cannot be performed in the laboratory, so the numerical simulation

provides the missing link between thermodynamic ideas and diffusion-mobility checks. □

Methods

Microscopic model

In the simulations, two grains in contact interact via a normal Hertz force, F_n, and a tangential Mindlin force F_t (ref. 12). For two spherical grains with radii R_1 and R_2: $F_n = \frac{2}{3} k_n R^{1/2} w^{3/2}$, $\Delta F_t = k_t (Rw)^{1/2} \Delta s$. Here $R = 2R_1 R_2/(R_1 + R_2)$, the normal overlap is $w = (1/2)[(R_1 + R_2) - |\mathbf{x}_1 - \mathbf{x}_2|] > 0$, where $\mathbf{x}_1$, $\mathbf{x}_2$ are the positions of the grain centres. The normal force acts only in compression, $F_n = 0$ when $w < 0$. The variable s is defined such that the relative shear displacement between the two grain centres is $2s$. The prefactors $k_n = 4G/(1 - \nu)$ and $k_t = 8G/(2 - \nu)$ are defined in terms of the shear modulus G and the Poisson's ratio ν of the material from which the grains are made (typically $G = 29$ GPa and $\nu = 0.2$, for glass beads). When F_t exceeds the Coulomb threshold, μF_n, the grains slide and $F_t = \mu F_n$, where μ is the friction coefficient between the spheres (typically $\mu = 0.3$). We assume a distribution of grain radii in which $R_1 = 0.105$ mm for half the grains and $R_2 = 0.075$ mm for the other half. The observables are measured in reduced units: length in units of R, force in units of GR^2, time in units of $\sqrt{\rho R^2/G}$, where ρ is the density of the particles.

MD simulations

We perform MD simulations for a system of 200 particles. Our calculations begin with a numerical protocol designed to mimic the experimental procedure used to prepare dense packed granular materials[15]. The simulations begin with a gas of spherical particles located at random positions in a periodically repeated cubic cell of side L. The system is then compressed and extended slowly until a specified value of the pressure and volume fraction—above the random close packing fraction—is achieved at static equilibrium. We then apply a gentle shear in the y-direction at constant volume by moving the periodic images at the top and bottom of the cell with velocities $\dot{\gamma} L/2$, where $\dot{\gamma}$ is the shear rate (Lees–Edwards boundary conditions) and using a suitable modified set of equations (see ch. 8 of ref. 16, and ref. 23) to generate a linear uniform shear velocity profile along the z-direction. Periodic boundary conditions are enforced in the x-direction and in the y-direction of the flow. We checked that shear-induced segregation is absent at the timescales of our simulations.

1. Edwards, S. F. in *Granular Matter: An Interdisciplinary Approach* (ed. Mehta, A.) 121–140 (Springer, New York, 1994).
2. Edwards, S. F. in *Disorder in Condensed Matter Physics* (eds Blackman, J. & Taguena, J.) 147–154 (Oxford Univ. Press, Oxford, 1991).
3. Mehta, A. & Edwards, S. F. Statistical mechanics of powder mixtures. *Physica A* **157**, 1091–1097 (1989).
4. Cugliandolo, L. F., Kurchan, J. & Peliti, L. Energy flow, partial equilibration, and effective temperatures in systems with slow dynamics. *Phys. Rev. E* **55**, 3898–3914 (1997).
5. Kurchan, J. in *Jamming and Rheology: Constrained Dynamics on Microscopic and Macroscopic Scales* (eds Liu, A. & Nagel, S. R.) 72–79 (Taylor and Francis, London, 2001).
6. Nicodemi, M. Dynamical response functions in models of vibrated granular media. *Phys. Rev. Lett.* **82**, 3734–3737 (1999).
7. Barrat, A., Kurchan, J., Loreto, V. & Sellitto, M. Edwards measures for powders and glasses. *Phys. Rev. Lett.* **85**, 5034–5037 (2000).
8. Javier Brey, J., Prados, A. & Sanchez-Rey, B. Thermodynamic description in a simple model for granular compaction. *Physica A* **275**, 310–324 (2000).
9. Lefevre, A. & Dean, D. S. Tapping spin-glasses and ferromagnets on random graphs. *Phys. Rev. Lett.* **86**, 5639–5642 (2001).
10. Sciortino, F. & Tartaglia, P. Extension of the fluctuation-dissipation theorem to the physical aging of a model glass-forming liquid. *Phys. Rev. Lett.* **86**, 107–110 (2001).
11. Nowak, E. R., Knight, J. B., Ben-Naim, E., Jaeger, H. M. & Nagel, S. R. Density fluctuations in vibrated granular materials. *Phys. Rev. E* **57**, 1971–1974 (1998).
12. Johnson, K. L. *Contact Mechanics* (Cambridge Univ. Press, Cambridge, 1985).
13. Cundall, P. A. & Strack, O. D. L. A Discrete numerical model for granular assemblies. *Géotechnique* **29**, 47–65 (1979).
14. Schäfer, J., Dippel, S. & Wolf, D. E. Force schemes in simulations of granular materials. *J. Phys. I (France)* **6**, 5–20 (1996).
15. Makse, H. A., Johnson, D. L. & Schwartz, L. M. Packing of compressible granular materials. *Phys. Rev. Lett.* **84**, 4160–4163 (2000).
16. Allen, M. P. & Tildesley, D. J. *Computer Simulations of Liquids* (Clarendon, Oxford, 1987).
17. Savage, S. B. The mechanics of rapid granular flows. *Adv. Appl. Mech.* **24**, 289–365 (1994).
18. Durian, D. J. Foam mechanics at the bubble scale. *Phys. Rev. Lett.* **75**, 4780–4783 (1995).
19. Lacasse, M.-D., Grest, G. S., Levine, D., Mason, T. G. & Weitz, D. A. Model for the elasticity of compressed emulsions. *Phys. Rev. Lett.* **76**, 3448–3451 (1996).
20. Langer, S. A. & Liu, A. J. Sheared foam as a supercooled liquid? *Europhys. Lett.* **49**, 68–73 (2000).
21. Herrmann, H. J., Hovi, J. P. & Luding, S. (eds) *Physics of Dry Granular Matter* (Kluwer, Dordrecht, 1998).
22. Ottino, J. M. & Khakhar, D. V. Mixing and segregation of granular materials. *Annu. Rev. Fluid Mech.* **32**, 55–91 (2000).
23. Hoover, W. G. *et al.* Lennard-Jones triple-point bulk and shear viscosities. Green-Kubo theory, Hamiltonian mechanics, and non-equilibrium molecular dynamics. *Phys. Rev. A* **22**, 1690–1697 (1980).
24. Drescher, A. & de Josselin de Jong, G. Photoelastic verification of a numerical model for the flow of a granular material. *J. Mech. Phys. Solids* **20**, 337–351 (1972).
25. Liu, C.-H. *et al.* Force fluctuations in bead packs. *Science* **269**, 513–515 (1995).
26. Jaeger, H. M., Nagel, S. R. & Behringer, R. P. Granular solids, liquids, and gases. *Rev. Mod. Phys.* **68**, 1259–1273 (1996).

....

Growth of nanowire superlattice structures for nanoscale photonics and electronics

Mark S. Gudiksen*†, **Lincoln J. Lauhon***†, **Jianfang Wang***,
David C. Smith*‡ & **Charles M. Lieber***§

* *Department of Chemistry and Chemical Biology, § Division of Engineering and Applied Sciences, Harvard University, Cambridge, Massachusetts 02138, USA*
† *These authors contributed equally to this work*

....

The assembly of semiconductor nanowires and carbon nanotubes into nanoscale devices and circuits could enable diverse applications in nanoelectronics and photonics[1]. Individual semiconducting nanowires have already been configured as field-effect transistors[2], photodetectors[3] and bio/chemical sensors[4]. More sophisticated light-emitting diodes[5] (LEDs) and complementary and diode logic[6–8] devices have been realized using both n- and p-type semiconducting nanowires or nanotubes. The n- and p-type materials have been incorporated in these latter devices either by crossing p- and n-type nanowires[2,5,6,9] or by lithographically defining distinct p- and n-type regions in nanotubes[8,10], although both strategies limit device complexity. In the planar semiconductor industry, intricate n- and p-type and more generally compositionally modulated (that is, superlattice) structures are used to enable versatile electronic and photonic functions. Here we demonstrate the synthesis of semiconductor nanowire superlattices from group III–V and group IV materials. (The superlattices are created within the nanowires by repeated modulation of the vapour-phase semiconductor reactants during growth of the wires.) Compositionally modulated superlattices consisting of 2 to 21 layers of GaAs and GaP have been prepared. Furthermore, n-Si/p-Si and n-InP/p-InP modulation doped nanowires have been synthesized. Single-nanowire photoluminescence, electrical transport and electroluminescence measurements show the unique photonic and electronic properties of these nanowire superlattices, and suggest potential applications ranging from nano-barcodes to polarized nanoscale LEDs.

Our approach to superlattice growth (Fig. 1) exploits recent developments in metal-catalysed nanowire synthesis, which have shown that nearly monodisperse metal nanoclusters can be used to control the diameter[11,12] and (through growth time) the length[13] of group III–V and group IV semiconductor nanowires by way of a vapour–liquid–solid growth process[14]. We introduce the vapour-phase semiconductor reactants required for nanowire growth by either laser ablation of solid targets[15,16] or vapour-phase molecular species[12,17]. To create a single junction within the nanowire, the addition of the first reactant is stopped during growth, and then a second reactant is introduced for the remainder of the synthesis (Fig. 1b); repeated modulation of the reactants during growth produces nanowire superlattices (Fig. 1c). In principle, this approach can be successfully implemented if a nanocluster catalyst suitable for growth of the different superlattice components under similar conditions is found; our previous studies[16] suggest that Au nanoclusters meet this requirement for a wide range of III–V and IV materials.

Gallium arsenide (GaAs)/gallium phosphide (GaP) superlattices have been grown by laser-assisted catalytic growth using GaAs and GaP targets. Figure 2 shows transmission electron microscopy (TEM) images of the products of this synthesis. It is relatively straightforward to focus on the junction area as the nanowire lengths can be controlled directly by growth times[13]. High-resolution TEM images of a typical GaAs/GaP junction region (Fig. 2a) exhibit a crystalline nanowire core without obvious defects, and show that the nanowire axes lies along the $\langle 111 \rangle$ direction, in agreement with previous studies of single-component systems[11,13,15,16]. Two-dimensional Fourier transforms calculated from high-resolution images containing the junction region (Fig. 2a, inset) show pairs of reciprocal lattice peaks along the different lattice directions, while such transforms calculated from the regions above and below the junction (not shown) exhibit only single reciprocal lattice peaks. Analysis of these peak data yield lattice constants, indexed to the zinc blende structures of GaP and GaAs, of 0.5474 ± 0.0073 nm and 0.5668 ± 0.0085 nm, and are in good agreement with the values for both GaP (0.5451 nm) and GaAs (0.5653 nm), respectively.

The TEM structural data suggest that the GaP/GaAs junctions could be abrupt, and thus we have carried out local elemental mapping of the heterojunction by energy dispersive X-ray spectroscopy (EDS) to address composition variation across the junction (Fig. 2b–e). These elemental maps show that Ga is uniformly distributed along the length of the nanowire, while P (Fig. 2d) and As (Fig. 2e) appear localized in the GaP and GaAs portions of the nanowire heterostructure, respectively. Quantitative analysis of the P and As composition variation (Fig. 2f) shows, however, that the junction is not atomically abrupt, but rather makes the transition between GaP and GaAs phases over a length scale of 15–20 nm. This length scale is reasonable considering that the ~20-nm-diameter Au catalyst must re-alloy with GaP after initial GaAs growth. The observed composition variation has several potentially important implications. First, composition variation at the interface can relieve strain, and may enable the defect-free junctions and superlattices that we observe in this system—which has a relatively large lattice mismatch. We note, however, that simple estimates of the length between dislocations (M.S.G. and C.M.L., unpublished results) suggest that defect-free, atomically abrupt interfaces may be possible in wires of diameter less than 20 nm. Second, there are photonic and electronic applications where abrupt interfaces are important. The observed composition variation could be substantially reduced in smaller-diameter nanowires; that is, a 5-nm-
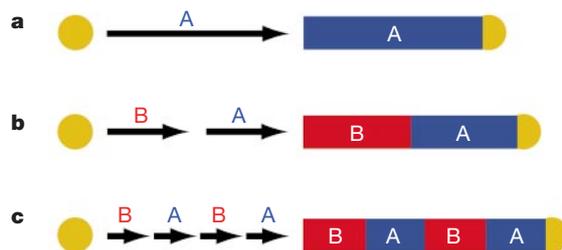

Figure 1 Synthesis of nanowire superlattices. **a**, A nanocluster catalyst (shown gold) nucleates and directs one-dimensional semiconductor nanowire (blue) growth with the catalyst remaining at the terminus of the nanowire. **b**, Upon completion of the first growth step, a different material (red) can be grown from the end of the nanowire. **c**, Repetition of steps **a** and **b** leads to a compositional superlattice within a single nanowire.

617